Hindawi
Shock and Vibration
Volume 2019, Article ID 9643124, 10 pages
https://doi.org/10.1155/2019/9643124

Research Article

Nonlinear Dynamic Analysis and Chaos Prediction of Grinding Motorized Spindle System

Weitao Jia,[1,2] **Feng Gao**,[1,2] **Yan Li**,[1,2] **Wenwu Wu**,[1,2] **and Zhongwei Li**[1,2]

[1]*Key Lab. of NC Machine Tools and Integrated Manufacturing Equipment of the Ministry of Education, Xi'an University of Technology, Xi'an 710048, Shaanxi, China*
[2]*Key Lab. of Manufacturing Equipment of Shaanxi Province, Xi'an University of Technology, Xi'an 710048, Shaanxi, China*

Correspondence should be addressed to Feng Gao; gf2713@126.com

Received 1 July 2019; Revised 16 August 2019; Accepted 28 August 2019; Published 22 September 2019

Academic Editor: Angelo Marcelo Tusset

The paper determines the impact factors of dynamics of a motorized spindle rotor system due to high speed: centrifugal force and bearing stiffness softening. A nonlinear dynamic model of the grinding motorized spindle system considering the above impact factors is constructed. Through system simulation including phase portraits and Poincaré map, the periodic behavior and chaotic behavior of the nonlinear grinding motorized spindle system are revealed. The threshold curve of chaos motion is obtained through the Melnikov method. The conclusion can provide a theoretical basis for researching deeply the dynamic behaviors of the grinding motorized spindle system.

1. Introduction

Although grinding motorized spindle machining technology has been widely used in ultraprecision and high-speed machine tools that can realize high-speed ultraprecision machining at a low cost, improvement of stability is still an important subject [1]. The unbalance of rotor mass is the main factor affecting the dynamic behavior of the motorized spindle system. The instability of the system results in abnormal operation, serious damage, and even "axle holding" [2, 3]. Therefore, analyzing the stability and predicting the threshold curve of chaos motion of motorized spindle system are necessary.

In engineering practice, there is still the unbalance of rotor mass. Many scholars have conducted in-depth research on this. The studies showed that dynamic characteristics of the system are related to the unbalance of rotor mass [4–7]. Huihui and Shuyun [8, 9], taking water lubricated motorized spindle as the research object, analyzed the dynamic behavior of the motorized spindle system under the coupling action of the unbalance of rotor mass and bearing tilt effect are studied. Bo et al. [10] investigated the dynamic performance of motorized spindle system under centrifugal force and bearing stiffness softening. The results display that the dynamic behavior of the system is affected seriously by the two factors and must be taken into account when modeling the motorized spindle system.

Under the high-speed running state, the rigidity of the motorized spindle bearing is softened to some extent. The centrifugal force of the spindle is the main influencing factor of the stiffness softening of the motorized spindle in the existing literature [11–15].

The dynamic model established from practical problem is generally nonlinear, and the system has complex dynamic behavior. Chaos is one of the unique phenomena of nonlinear systems. Along with the progress of nonlinear dynamics, nonlinear behaviors of the system such as stability solution, periodic solution, bifurcation, and chaos, have become hot internet topic. Many scholars have focused on rotor bearing system models, and the main methods for analyzing the dynamic behavior of nonlinear systems include axis orbit, power spectra, phase portraits, Poincare map, and bifurcation diagrams. The modeling results can predict the stability parameters of the rotor bearing system and avoid the range of unstable motion of the rotor bearing system [16–20].

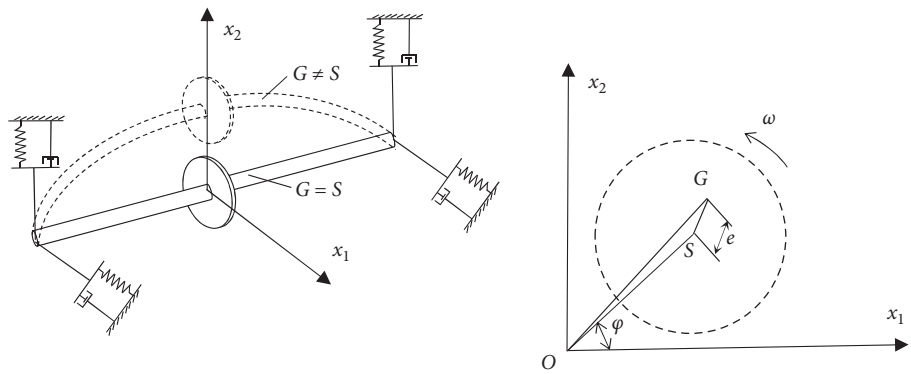

Figure 1: Diagram of the motorized spindle system.

Li et al. [21] & Sheu et al. [22] investigated the nonlinear dynamics of Duffing system. The nonlinear dynamic characteristics of the Duffing system are researched by time-domain diagram, phase portraits, Poincaré map, and bifurcation diagrams.

At present, numerical analysis is mainly used to study nonlinear dynamics, but it cannot provide the analytic solution of the nonlinear system. Melnikov method proposed a new and more applicable method of chaos criterion, and proved its effectiveness by solving nonlinear system described through the Duffing equation. Because of the effectiveness of Melnikov method, many scholars are still applying it nowadays. Yagasaki [23] & Zhang et al. [24] utilized the Melnikov method, and the research show that abundant bifurcation behavior and chaos motions occur in vibrations of the microcantilever. Yu et al. [25, 26] investigated nonlinear dynamics of a flexible rotor system, and obtained the parameter range of the occurrence of chaos motion in the sense of Smale horseshoes. Siewe et al. [27, 28] et al. obtained the condition of heteroclinic and homoclinic chaos of Rayleigh and Van der Pol oscillator by applying Melnikov method. Zhang and Zhou [29] investigated the chaotic behaviors of a nanoplate by the Melnikov method. The threshold curve of chaotic motion is given. Jibin and Fengjuan [30], Liu et al. [31], and Li et al. [32] gave the critical parameter curve of the Duffing oscillator for the existence of chaos in the Smale horse sense by Melnikov method.

At high speed, bearing softening will occur, which strongly affects the dynamic behavior of motorized spindle system. However, in previous literatures, the study of bearing softening effect is relatively rare, mainly considering the system as a hard spring system. The novelty of this paper is to consider the effect of bearing softening on the motorized spindle system.

This article established the nonlinear dynamic model of the nonlinearly supported motorized spindle rotor bearing system under centrifugal force and bearing stiffness softening. The nonlinear characteristics of motorized spindle system are shown using phase portraits and Poincaré map by means of numerical analysis. The threshold curve of motorized spindle system is obtained under periodic perturbation through Melnikov method. The results could be used to design and optimize motorized spindle system, and it is of practical significance for the purpose of guaranteeing system stability.

2. Mathematical Formulation

The stiffness and damping of motorized spindle system may be influenced such as bearing, pedestal, and so on. The model of motorized spindle system is as follows:

The rotor bearing model with nonlinear support is established by equivalent spring and damping. Then, the nonlinear dynamics equation of motorized spindle system under centrifugal force is as follows:

$$\begin{cases} m\ddot{x}_1 + c\dot{x}_1 + k_1 x_1 + k_3 x_1^3 = me\omega^2 \cos(\omega t), \\ m\ddot{x}_2 + c\dot{x}_2 + k_1 x_2 + k_3 x_2^3 = me\omega^2 \sin(\omega t), \end{cases} \tag{1}$$

where m, e, and ω are mass of the rotor, mass eccentricity, and rotating speed, respectively. c, k_1, and k_3 denote damping, linear, and nonlinear stiffness of bearing.

Since there is no coupling term between the first and the second formulas in equation (1), the vibration of each degree of freedom is relatively independent, and the vibration in x_2 direction is the same as that in x_1, but there is only a phase difference, so in this paper, only one of the equations needs to be investigated.

The high-speed grinding motorized spindle system is a kind of electromechanical coupling system. The rotor bearing system exhibits soft characteristics; therefore, $a < 0$.

The first of equation (1) is rewritten as

$$\ddot{x}_1 + \xi\dot{x}_1 + \omega_n^2 x_1 - \widehat{a}x_1^3 = e\omega^2 \cos(\omega t), \tag{2}$$

where $\xi = c/m$ and $\widehat{a} = |k_3|/m$.

One can rewrite the equation of motion (2) in the dimensionless form as [30]

$$\ddot{y} + r\dot{y} + y - y^3 = f\cos(\lambda\tau), \tag{3}$$

where the dimensionless parameters are $y = kx_1$, $k = \sqrt{\widehat{a}/\omega_n^2}$, $\tau = \omega_n t$, $r = \xi/\omega_n$, $f = e\omega^2\sqrt{\widehat{a}}/\omega_n^3$, and $\lambda = \omega/\omega_n$.

For the rotor bearing system of high-speed grinding motorized spindle, $r << 1$, $f << 1$, so r, f is regarded as a small parameter. Equation (3) is the Duffing equation with weak periodic forced oscillation equation.

3. Simulation Analysis

Phase portraits and Poincaré map are obtained by using displacement and velocity of system response as horizontal

and longitudinal coordinates. That is to say horizontal coordinates is displacement, and longitudinal coordinates is velocity. Poincare diagram is obtained by sampling every rotation cycle. If the response of the system is periodic n, there are n isolated points on Poincaré map. If the system is periodic motion, it presents a closed curve. If the system is chaotic motion, it is a disordered point.

The Runge–Kutta method is used to solve the differential equation of the system. Taking 150MD24Z7.5 high-speed grinding motorized spindle for example, the motorized spindle system is found to display intricate dynamics characteristics.

3.1. Response of the System at Different Rotational Speeds for $e = 0.001$ mm, $k_1 = 2.2488 \times 10^9$ N/m. Phase portraits and Poincaré map of the system are shown in Figures 2–6, respectively, ω as the control parameter.

When the speed is 3000 r/min, it can be seen from Figure 2(a) that the phase portraits form a closed curve, and there are three isolated points in the Poincaré map; then the system is period-3(P3) motion.

In the same way, when the speed reaches 5000 r/min, there are eleven isolated points in Poincaré map the system is period-11(P11) motion.

When the speed is 10000 r/min, phase portraits form a complex curve, and there are a lot of disordered points in the Poincaré map. Thus, the system is in chaotic motion.

In the same way, when the speed is 15000 r/min, the system is still in chaotic motion.

As the rotational speed continues to increase, when the speed reaches 20000 r/min, and there are two points in Poincaré map, the system returns to period-2(P2) motion.

It can be seen from Figures 2–6 that when the rotation speed is 3000 r/min, 5000 r/min, or 20000 r/min, phase portraits form a closed figure. When the rotating speed is 10000 r/min or 15000 r/min, phase portraits are irregular curves. From the Poincaré map, it takes the general form (P3 ⟶ P11 ⟶ chaos ⟶ P2) with the change of rotational speed between the values (3000 r/min~20000 r/min).

3.2. Response of the System at Different Rotational Speeds for $e = 0.001$ mm, $k_1 = 2.2488 \times 10^{10}$ N/m. Phase portraits and Poincaré map of the system are shown in Figures 7–11, respectively, with ω as the control parameter.

When the speed is 3000 r/min, it can be seen from Figure 7(a) that the phase portraits is a closed curve, and there is one point in the Poincaré map; then the dynamic response undergoes synchronous vibration with period-1(P1) motion.

In the same way, when the speed is 5000 r/min, the system is still in period-1(P1) motion.

When the speed increases to 10000 r/min, as can be seen from Figure 7, and there are seven points in Poincaré map, the system is in period-7(P7) motion.

Similarly, when the speed is 15000 r/min, the system is still in period-3(P3) motion.

It is obvious that when the speed is 20000 r/min, there are countable points, so the system is in period-n(P-n) motion.

It can be seen from Figures 7–11, no matter what the speed is, phase portraits form a closed figure. Thus, the system has gone through a process (P1 ⟶ P7 ⟶ P3 ⟶ P-n) from the Poincaré map when the rotating speed varied from 3000 r/min to 20000 r/min.

In short, the nonlinear characteristics of the motorized spindle system are shown in Table 1 synthetically.

In Table 1, when $k_1 = 2.2488 \times 10^9$, the nonlinear characteristics of motorized spindle system have undergone different stages as the rotating speed varied, from periodic to chaotic, and finally back to periodic; when $k_1 = 2.2488 \times 10^{10}$, the system is periodic motion. As shown in Figures 2–11, with the increase of stiffness, it can be seen that the stiffness suppresses the occurrence of chaos, improving the vibration behavior for rotor bearing system of grinding motorized spindle.

4. Chaotic Prediction

The research and application of chaos theory has been extended to many fields such as natural science and social science and has become an important part o f modern nonlinear system theory. With the deepening of scientific research, the status of prediction is particularly prominent. In this paper, the Melnikov method is used to predict the threshold of the occurrence of chaos motion [27, 28].

Equation (3) is the Duffing equation with weak periodic forced oscillation equation. Then, the chaotic threshold of rotor bearing system of grinding motorized spindle is studied based on the Melnikov method.

The systems shown in equation (3) are equivalent to

$$\begin{cases} \dot{y} = z, \\ \dot{z} = -y + y^3 + \varepsilon(-r\dot{y} + f\cos(\lambda\tau)). \end{cases} \tag{4}$$

Equation (4) is written in matrix form:

$$\dot{Y} = f(Y) + \varepsilon g(Y, t), \tag{5}$$

where $Y = (y, z)^T$, $f(Y) = (z, -y + y^3)^T$, and $g(Y, t) = (0, -ry' + f\cos(\lambda\tau))^T$.

When $\varepsilon = 0$, the unperturbed system is

$$\begin{cases} \dot{y} = z, \\ \dot{z} = -y + y^3. \end{cases} \tag{6}$$

The system of (6) is a Hamilton system with a potential function

$$U(x) = \frac{y^2}{2} - \frac{y^4}{4}. \tag{7}$$

Obviously, this is a single-well system. The potential energy surface of the system in the three-dimensional phase space and the potential energy function on the plane are shown in Figure 12.

The Hamilton function of the unperturbed is given by

$$H(y, z) = \frac{1}{2}z^2 + \frac{1}{2}y^2 - \frac{1}{4}y^2 = h. \tag{8}$$

The Hamilton function of the unperturbed is shown in Figure 13.

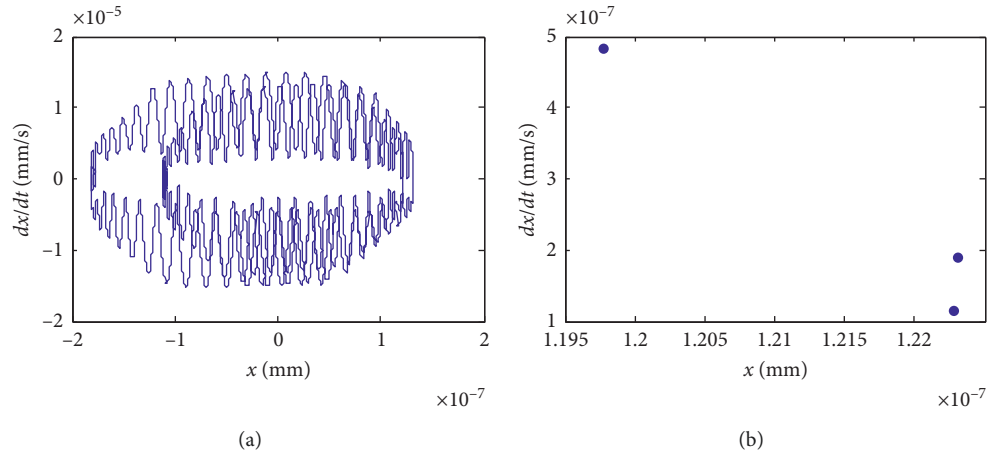

Figure 2: System response for $\omega = 3000$ r/min. (a) Phase portraits. (b) Poincaré map.

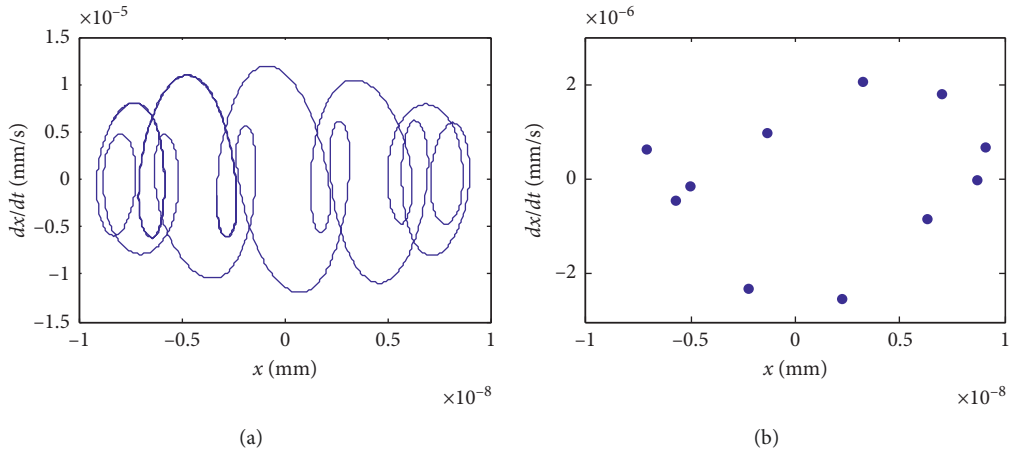

Figure 3: System response for $\omega = 5000$ r/min. (a) Phase portraits. (b) Poincaré map.

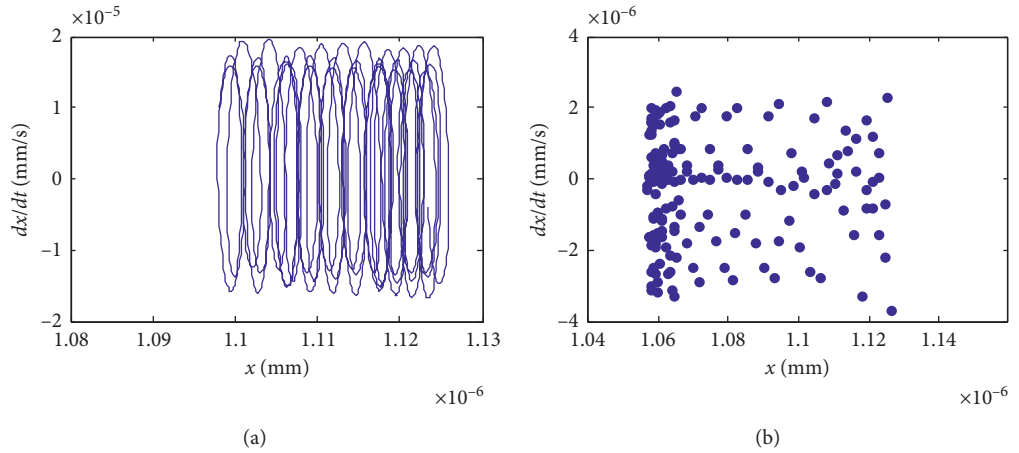

Figure 4: System response for $\omega = 10000$ r/min. (a) Phase portraits. (b) Poincaré map.

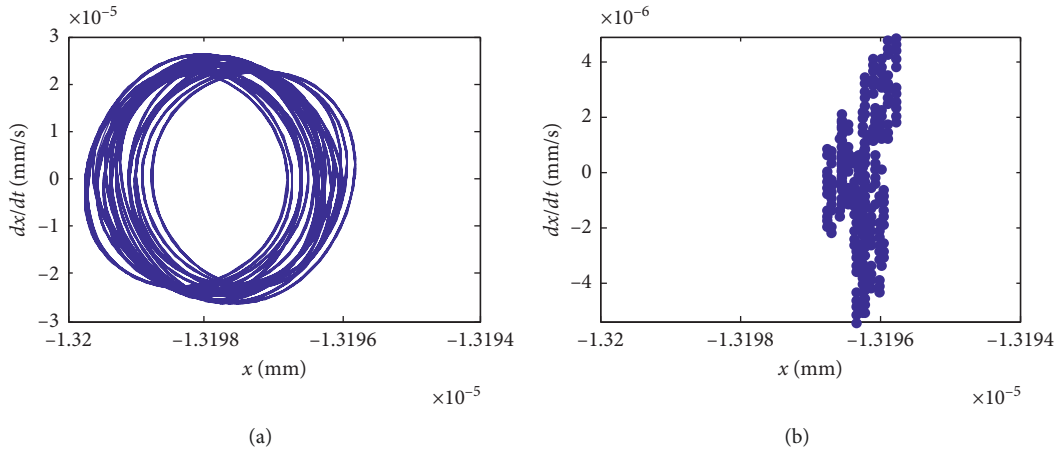

Figure 5: System response for $\omega = 15000$ r/min. (a) Phase portraits. (b) Poincaré map.

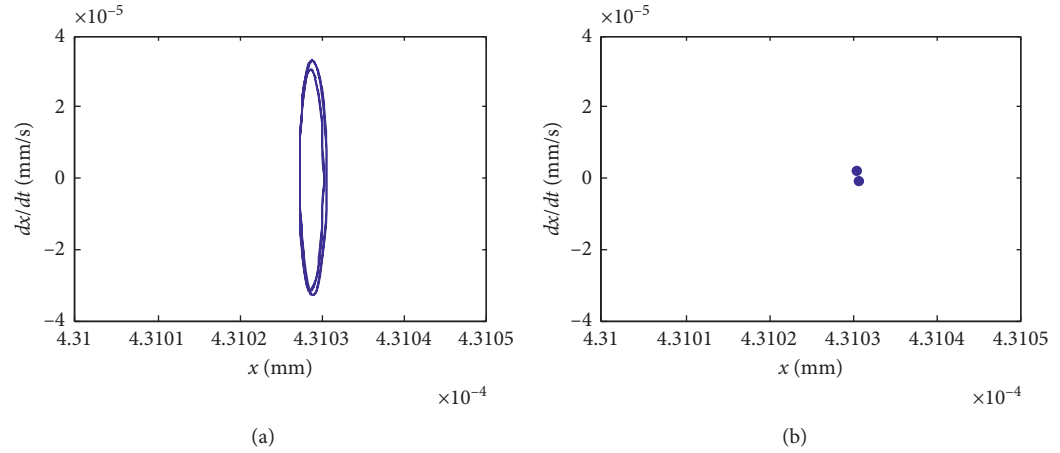

Figure 6: System response for $\omega = 20000$ r/min. (a) Phase portraits. (b) Poincaré map.

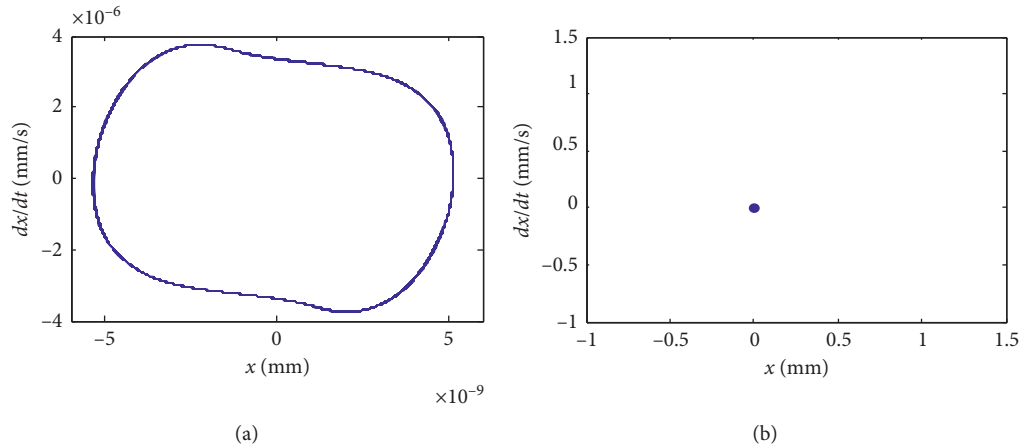

Figure 7: System response for $\omega = 3000$ r/min. (a) Phase portraits. (b) Poincaré map.

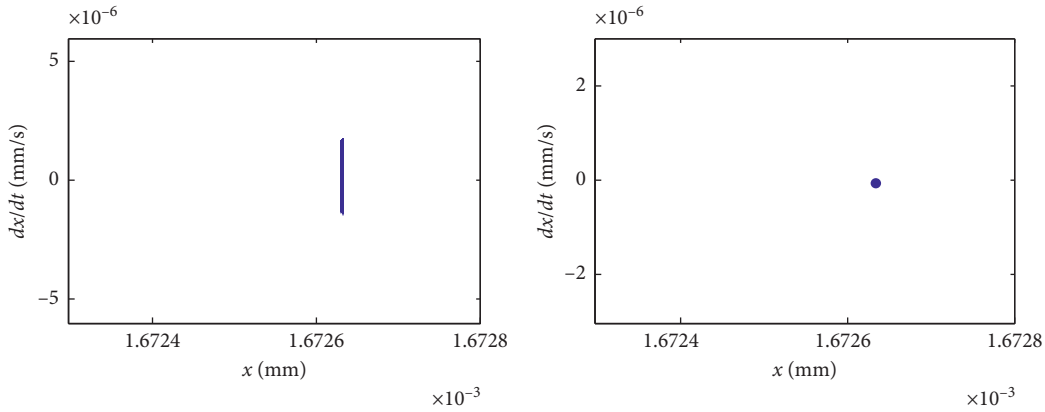

Figure 8: System response for $\omega = 5000$ r/min. (a) Phase portraits. (b) Poincaré map.

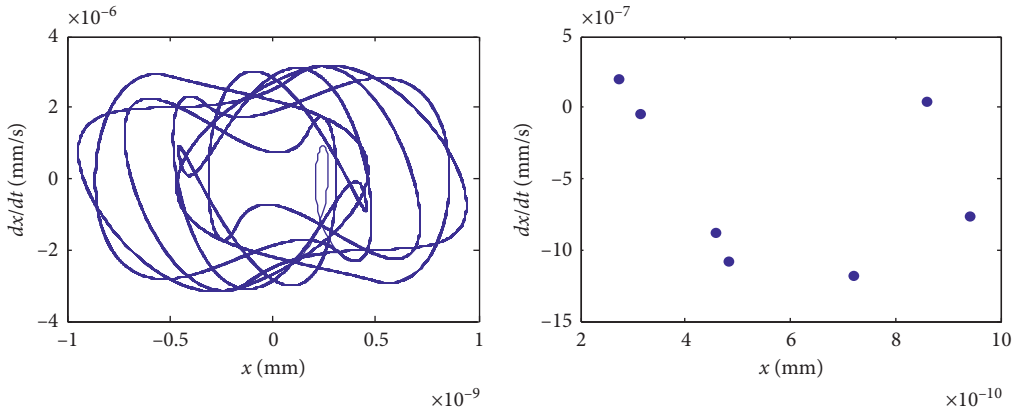

Figure 9: System response for $\omega = 10000$ r/min. (a) Phase portraits. (b) Poincaré map.

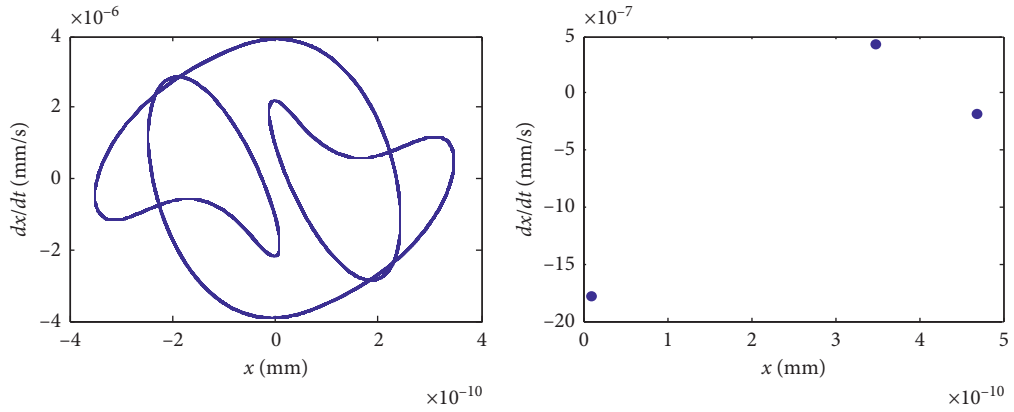

Figure 10: System response for $\omega = 15000$ r/min. (a) Phase portraits. (b) Poincaré map.

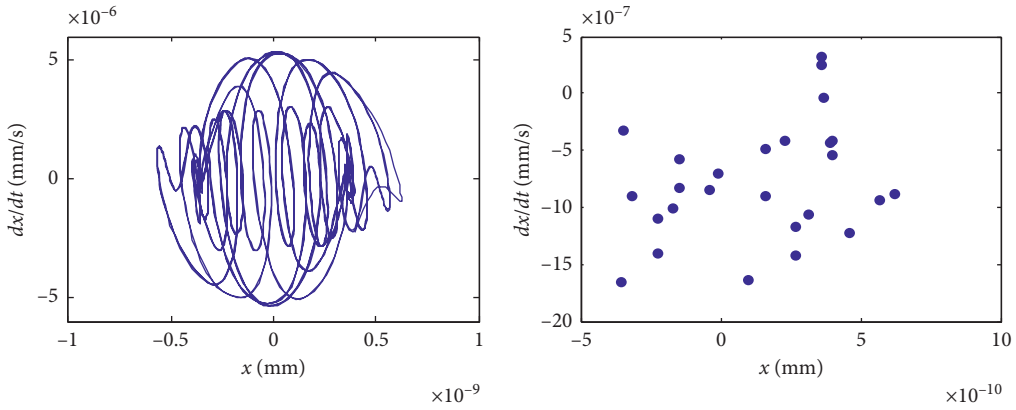

Figure 11: System response for $\omega = 20000$ r/min. (a) Phase portraits. (b) Poincaré map.

Table 1: Motion characteristics of the motorized spindle.

r/min	k_1 (N/m)	
	2.2488×10^9	2.2488×10^{10}
3000	P3	P1
5000	P11	P1
10000	Chaos	P7
15000	Chaos	P3
20000	P2	P-n

The characteristic equation of the linear approximation system $\lambda'^2 + 1 = 0$, its characteristic root is $\lambda'_{1,2} = \pm i$; therefore, (0, 0) is the center, while (1, 0) and (−1, 0) are singularity. The characteristic equation is:

$$\begin{vmatrix} 0 - \lambda' & 1 \\ -1 + 3y^2 & 0 - \lambda' \end{vmatrix} = 0. \tag{9}$$

So $\lambda'_{1,2} = \pm\sqrt{2}$, (1, 0) and (−1, 0) are saddle points. When $h = 1/4$, there are two heteroclinic trajectories connected to (1, 0) and (−1, 0), and these two trajectories make up a heteroclinic circle. When $0 < h < 1/4$, there is a closed loop surrounded by a family of (0, 0), as shown in Figure 14.

By integrating, the parameter equations of two heteroclinic trajectories are obtained:

$$\begin{cases} y_{\pm}^0(t) = \pm th\left(\dfrac{\sqrt{2}}{2}t\right), \\ z_{\pm}^0(t) = \pm\dfrac{\sqrt{2}}{2}\sec h^2\left(\dfrac{\sqrt{2}}{2}t\right). \end{cases} \tag{10}$$

The corresponding Melnikov functions are as follows:

$$M_{\pm}(t_0) = \int_{-\infty}^{+\infty} f\left(q_i^0(t)\right) \wedge g\left(q_i^0(t), t + t_0\right) dt, \tag{11}$$

where

$$\begin{aligned} q_i^0(t) &= \begin{pmatrix} y_{\pm}^0(t) \\ z_{\pm}^0(t) \end{pmatrix}, \\ f\left(q_i^0(t)\right) &= \begin{pmatrix} z_{\pm}^0(t) \\ -y_{\pm}^0(t) + \left[y_{\pm}^0(t)\right]^3 \end{pmatrix}, \\ g\left(q_i^0(t), t + t_0\right) &= \begin{pmatrix} 0 \\ -rz_{\pm}^0(t) + f\cos\left(\lambda\left(t + t_0\right)\right) \end{pmatrix}, \\ f\left(q_i^0(t)\right) \wedge g\left(q_i^0(t), t + t_0\right) &= \begin{pmatrix} y_{\pm}^0(t) - \left[y_{\pm}^0(t)\right]^3 \\ z_{\pm}^0(t) \end{pmatrix} \cdot \begin{pmatrix} 0 \\ -rz_{\pm}^0(t) + f\cos\left(\lambda\left(t + t_0\right)\right) \end{pmatrix} \\ &= \left[-rz_{\pm}^0(t) + f\cos\left(\lambda\left(t + t_0\right)\right)\right] z_{\pm}^0(t). \end{aligned} \tag{12}$$

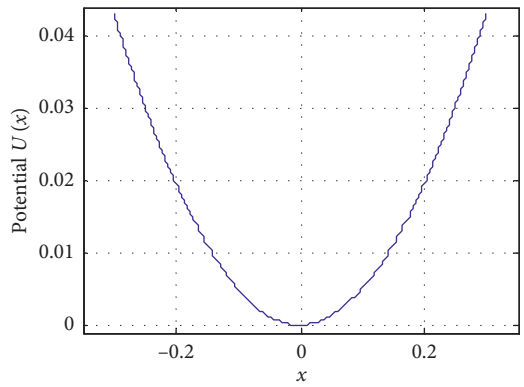

Figure 12: Potential function of the unperturbed system.

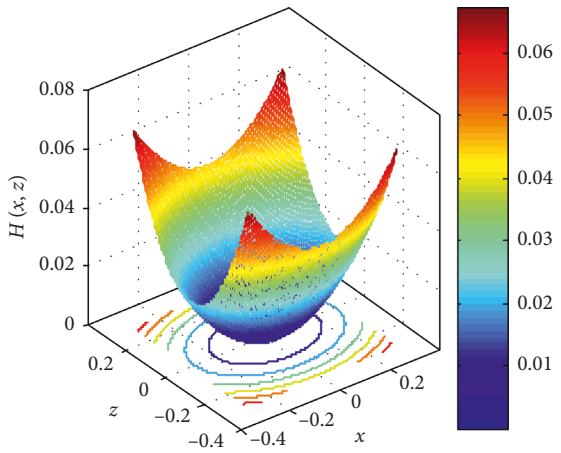

Figure 13: Hamilton function of the unperturbed system.

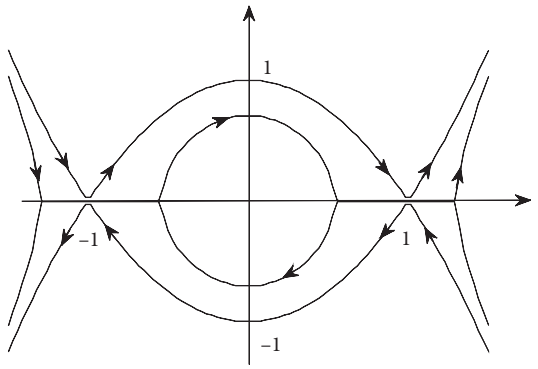

Figure 14: Phase portraits of rotor bearing system of grinding motorized spindle.

Therefore,

$$M_{\pm}(t_0) = \int_{-\infty}^{+\infty} \left[-rz_{\pm}^{0}(t) + f\cos\left(\lambda\left(t + t_0\right)\right)\right] z_{\pm}^{0}(t)dt = rI_1 \pm fI_2\cos\left(\lambda t_0\right), \tag{13}$$

where $I_1 = 2/3$ and $I_2 = \pi\lambda \cosh(\pi\lambda/2)$.

Because $M \pm (t0) = 0$,

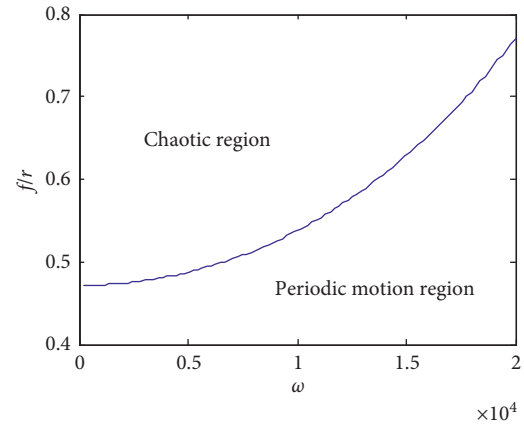

Figure 15: Melnikov function threshold curve of rotor bearing system of motorized spindle.

$$\cos\left(\omega t_0\right) = \pm\frac{rI_1}{fI_2}. \tag{14}$$

If the equation is solved, then

$$\frac{rI_1}{fI_2} < 1, \quad \text{that is } \frac{f}{r} > \frac{I_1}{I_2}, \tag{15}$$

Because $M'_{\pm}(t_0) = -\lambda f I_2 \sin\left(\lambda t_0^{\pm}\right) \cdot \neq 0$, then $M_{\pm}(t_0)$ has its single zero point; thus, the system is chaotic. Therefore, when the ratio of the parameter f to the r exceeds the threshold $2\sin h(\pi\lambda/\sqrt{2})/(3\pi\lambda)$, the system has chaos in the sense of Smale horseshoe.

The chaotic threshold of the rotor bearing system of grinding motorized spindle is shown in Figure 15.

5. Conclusion

In this article, a nonlinear dynamic model of grinding motorized spindle system considering centrifugal force and bearing stiffness softening has been proposed to research dynamical behavior and predict the threshold of chaos motion of system. Several results are as follows:

(1) Through the system simulation including phase portraits and Poincaré map, the periodic and chaotic behavior of grinding motorized spindle system are revealed as rotating speed increases.

(2) Comparing the dynamic behavior of the motorized spindle system under different stiffnesses, it is found that the system exhibits good nonlinearity as stiffness increases. At the same time, it is shown that the increase of system stiffness can suppress the occurrence of chaos.

(3) Using the Melnikov method, the threshold curve of chaos motion has been predicted. The results could be used to provide the theory basis for practical production.

The results could help engineers and researchers design and research the grinding motorized spindle system and provide a theoretical basis for further research about

complex nonlinear characteristics, selecting the range of system stable operating parameters.

Data Availability

The data used to support the findings of this study are included within the article.

Conflicts of Interest

The authors declare that there are no conflicts of interest regarding the publication of this paper.

Acknowledgments

The authors acknowledge support by the Shaanxi Provincial Key Research and Development Program (grant no. 2018ZDXM-GY-074) and Natural Science Basic Research Plan in Shaanxi Province of China (program no. 2019JM-148).

References

[1] X. Wanli, Y. Xuebing, L. Lang, and Y. Julong, "Review on key technology of hydrodynamic and hydrostatic high-frequency motor spindles," *Journal of Mechanical Engineering*, vol. 45, no. 9, pp. 1–18, 2009.

[2] X. Wanli, H. Zhiquan, L. Lang, and Y. Xuebing, "Review on the dynamic characteristics of aerostatic motorized spindles," *Journal of Mechanical Engineering*, vol. 47, no. 5, pp. 40–58, 2011.

[3] J. S. Larsen and I. F. Santos, "On the nonlinear steady-state response of rigid rotors supported by air foil bearings-theory and experiments," *Journal of Sound and Vibration*, vol. 346, pp. 284–297, 2015.

[4] L. Shusen, "Analysis of the dynamics of precision centrifuge spindle system with the externally pressurized gas bearing," *Chinese Journal of Mechanical Engineering*, vol. 41, no. 2, pp. 28–32, 2005.

[5] C. Dongju, F. Jinwei, and Z. Feihu, "Dynamic and static characteristics of a hydrostatic spindle for machine tools," *Journal of Manufacturing Systems*, vol. 31, no. 1, pp. 26–33, 2012.

[6] H. M. Navazi and M. Hojjati, "Nonlinear vibrations and stability analysis of a rotor on high-static-low-dynamic-stiffness supports using method of multiple scales," *Aerospace Science and Technology*, vol. 63, pp. 259–265, 2017.

[7] M. R. Rashidi, M. A. Karami, and B.-N. Firooz, "Numerical analysis of a rigid rotor supported by aerodynamic four-lobe journal bearing system with mass unbalance," *Communications in Nonlinear Science & Numerical Simulation*, vol. 17, no. 1, pp. 454–471, 2012.

[8] F. Huihui and J. Shuyun, "Dynamic analysis of water-lubricated motorized spindle considering tilting effect of thrust bearing," *Proceedings of the Institution of Mechanical Engineers, Part C Journal of Mechanical Engineering Science*, vol. 231, no. 20, pp. 3780–3790, 2016.

[9] F. Huihui and J. Shuyun, "Dynamics of a motorized spindle supported on water-lubricated bearings," *Proceedings of the Institution of Mechanical Engineers, Part C Journal of Mechanical Engineering Science*, vol. 231, no. 3, pp. 459–472, 2015.

[10] W. Bo, S. Wei, and W. Bang-Chun, "The effect of high speeds on dynamic characteristics of motorized spindle system," *Engineering Mechanics*, vol. 32, no. 6, pp. 231–237, 2015.

[11] J.-S. Chen and Y.-W. Hwang, "Centrifugal force induced dynamics of a motorized high-speed spindle," *The International Journal of Advanced Manufacturing Technology*, vol. 30, no. 1-2, pp. 10–19, 2006.

[12] C.-W. Lin, J. F. Tu, and J. Kamman, "An integrated thermo-mechanical-dynamic model to characterize motorized machine tool spindles during very high speed rotation," *International Journal of Machine Tools & Manufacture*, vol. 43, no. 10, pp. 1035–1050, 2003.

[13] J.-J. Sinou, "Non-linear dynamics and contacts of an unbalanced flexible rotor supported on ball bearings," *Mechanism and Machine Theory*, vol. 44, no. 9, pp. 1713–1732, 2009.

[14] C. Li and Z. Jianrong, "Nonlinear vibration and stability analysis of a flexible rotor supported on angular contact ball bearings," *Journal of Vibration and Control*, vol. 20, no. 12, pp. 1767–1782, 2014.

[15] C. Xing, Y. Shihua, and P. Zengxiong, "Nonlinear vibration for PMSM used in HEV considering mechanical and magnetic coupling effects," *Nonlinear Dynamics*, vol. 80, no. 1-2, pp. 541–552, 2015.

[16] C.-W. Chang-Jian, "Non-linear dynamic analysis of dual flexible rotors supported by long journal bearings," *Mechanism and Machine Theory*, vol. 45, no. 6, pp. 844–866, 2010.

[17] C.-W. Chang-Jian and C.-K. Chen, "Bifurcation and chaos analysis of a flexible rotor supported by turbulent long journal bearings," *Chaos, Solitons & Fractals*, vol. 34, no. 4, pp. 1160–1179, 2007.

[18] C.-W. Chang-Jian and C.-K. Chen, "Chaos and bifurcation of a flexible rotor supported by porous squeeze couple stress fluid film journal bearings with non-linear suspension," *Chaos, Solitons & Fractals*, vol. 35, no. 2, pp. 358–375, 2008.

[19] C.-W. Chang-Jian and C. O.-K. Chen, "Chaotic response and bifurcation analysis of a flexible rotor supported by porous and non-porous bearings with nonlinear suspension," *Nonlinear Analysis: Real World Applications*, vol. 10, no. 2, pp. 1114–1138, 2009.

[20] L. Xiang, A. Hu, L. Hou, Y. Xiong, and J. Xing, "Nonlinear coupled dynamics of an asymmetric double-disc rotor-bearing system under rub-impact and oil-film forces," *Applied Mathematical Modelling*, vol. 40, no. 7-8, pp. 4505–4523, 2016.

[21] Z. Li, D. Chen, J. Zhu, and Y. Liu, "Nonlinear dynamics of fractional order Duffing system," *Chaos, Solitons & Fractals*, vol. 81, pp. 111–116, 2015.

[22] L.-J. Sheu, H.-K. Chen, J.-H. Chen, and L.-M. Tam, "Chaotic dynamics of the fractionally damped Duffing equation," *Chaos, Solitons & Fractals*, vol. 32, no. 4, pp. 1459–1468, 2007.

[23] K. Yagasaki, "Bifurcations and chaos in vibrating micro-cantilevers of tapping mode atomic force microscopy," *International Journal of Non-linear Mechanics*, vol. 42, no. 4, pp. 658–672, 2007.

[24] W. Zhang, M. H. Yao, and J. H. Zhang, "Using the extended Melnikov method to study the multi-pulse global bifurcations and chaos of a cantilever beam," *Journal of Sound and Vibration*, vol. 319, no. 1-2, pp. 541–569, 2009.

[25] T.-J. Yu, S. Zhou, X.-D. Yang, and W. Zhang, "Global dynamics of a flexible asymmetrical rotor," *Nonlinear Dynamics*, vol. 91, no. 2, pp. 1041–1060, 2018.

[26] T.-J. Yu, W. Zhang, and X.-D. Yang, "Global bifurcations and chaotic motions of a flexible multi-beam structure," *International Journal of Non-linear Mechanics*, vol. 95, pp. 264–271, 2017.

[27] M. S. Siewe, H. Cao, and M. A. F. Sanjuán, "On the occurrence of chaos in a parametrically driven extended Rayleigh oscillator with three-well potential," *Chaos, Solitons & Fractals*, vol. 41, no. 2, pp. 772–782, 2009.

[28] M. S. Siewe, F. M. M. Kakmeni, C. Tchawoua, and P. Woafo, "Bifurcations and chaos in the triple-well -Van der Pol oscillator driven by external and parametric excitations," *Physica A: Statistical Mechanics and its Applications*, vol. 357, no. 3-4, pp. 383–396, 2005.

[29] X. Zhang and L. Zhou, "Melnikov's method for chaos of the nanoplate postulating nonlinear foundation," *Applied Mathematical Modelling*, vol. 61, pp. 744–749, 2018.

[30] L. Jibin and C. Fengjuan, *Chaos, Melnikov Method and New Development*, Science Press, Beijing, China, 2012.

[31] Z. R. Liu, W. G. Yao, and Z. X. Zhu, "Road to chaos for a soft spring system under weak periodic disturbance," *Applied Mathematics & Mechanics*, vol. 7, no. 2, pp. 111–116, 1986.

[32] H. Li, X. Liao, S. Ullah, and L. Xiao, "Analytical proof on the existence of chaos in a generalized Duffing-type oscillator with fractional-order deflection," *Nonlinear Analysis: Real World Applications*, vol. 13, no. 6, pp. 2724–2733, 2012.